Rotating billiards

1989 J. Phys. A: Math. Gen. 22 1765

(http://iopscience.iop.org/0305-4470/22/11/018)

J. Phys. A: Math. Gen. 22 (1989) 1765-1778. Printed in the UK

Rotating billiards

H Frisk†‡§ and R Arvieu†

† Institute des Sciences Nucléaires, 53 Avenue des Martyrs, 38026 Grenoble Cedex, France
‡ Department of Mathematical Physics, Lund Institute of Technology, 22100 Lund, Sweden

Received 1 November 1988

Abstract. The motion of a classical particle within a billiard which rotates uniformly in the counterclockwise sense around its centre is studied. In the case of an elliptical boundary the counterclockwise motion shows a notable stability while the clockwise motion is to a large extent chaotic when the motion along the boundary in the clockwise sense is not possible. The organisation of phase space for the rotating billiard and the billiard in a constant magnetic field studied by Robnik and Berry is similar for weak fields but clearly different for strong fields where the variable curvature for the rotating billiard is manifested. For strong inertial forces the rotating stadium and the rotating ellipse behave in a similar manner.

1. Introduction

The aim of this article is to provide a description of the classical phase space associated with trajectories of a free particle inside a billiard which rotates with constant angular frequency around an axis perpendicular to the billiard plane and through its centre. The billiards are considered as some of the simplest 'laboratories' which exhibit the richness of the phase space of classical mechanics and for which the connection between classical and quantum mechanics can be studied. Several mathematical results were already derived by Birkhoff (1927) and recent reviews of the subject have been given by Sinai (1976) and Berry (1981a). In the last ten years many numerical experiments have been published, by for example, Benettin and Strelcyn (1978), Berry (1981b), McDonald and Kaufman (1979, 1988), Henon and Wisdom (1983), Robnik (1983, 1984), Heller (1984) and Christoffel and Brumer (1986). A new class of billiards was introduced recently by Robnik and Berry (1985), namely billiards in constant magnetic fields. These systems with broken time-reversal symmetry belong to the universality class (Berry 1987) for which the statistics of the corresponding quantal eigenenergies is fitted by the ensemble of random complex Hermitian matrices. For an example see the Aharonov-Bohm billiard studied by Berry and Robnik (1986a, b).

The rotating billiard is not time-reversal invariant and has much in common with the billiard in a constant magnetic field. The former is the two-dimensional classical counterpart of the cranking model of Inglis (1956) which nuclear physicists use to analyse the nucleonic response to the rotation of the nuclear field (Bohr and Mottelson 1975) while the latter mimic the behaviour of electrons in a magnetic field and, for example, the connection between chaos and diamagnetism can be investigated

§ Present address: Niels Bohr Institute, University of Copenhagen, Blegdamsvej DK-2100 Copenhagen Ø, Denmark.

0305-4470/89/111765+14$02.50

(Nakamura and Thomas 1988). Since the Laplace force introduces a constant curvature for a constant magnetic field while the inertial forces in the rotating case generate several regimes of curvature, both systems have a value in their own right. Robnik and Berry (1985) showed the existence of a regime of locally integrable adiabatic skipping motion and a regime of chaotic flyaway orbits. The former event was proved mathematically by Lazutkin (1973) for a free particle in a plane convex domain with a sufficiently smooth boundary. The phase space of the billiard in a Coriolis-centrifugal field contains these two regimes but its organisation is different from the magnetic field case when then the fields are strong.

Fairlie and Siegwart (1988) were the first to consider a rotating billiard. They chose a circular table rotating uniformly about a point located on the edge and showed that the phase portrait of this system contains all the features of chaotic systems. Choosing instead an ellipse or a stadium rotating around its centre is a natural extension of previous studies, see Keller and Rubinow (1960) and Arvieu and Ayant (1987a, b) for the ellipse. The discussion by Fairlie and Siegwart will also be somewhat extended in our paper. The ellipse is finally the simplest possible model that must be solved before considering the rotation of a more realistic three-dimensional potential. Simple results on this latter system have already been derived by Bohr and Mottelson (1980) but the full problem has not yet been treated. In § 2 the motion of a free particle in a rotating system (no boundary) is examined. The boundary is taken into account in § 3. Some of the most important trajectories in a rotating ellipse are analysed in § 4 which facilitates the interpretation of the numerical experiments presented in § 5 for the ellipse and the stadium.

2. Trajectories in a rotating system of a free particle

Let us examine the different types of trajectories of a free particle which are obtained in a two-dimensional system rotating in the counterclockwise sense with a constant rotational frequency, ω. At $t=0$ the rotating axes are assumed to coincide with the fixed axes OX and OY and the particle is assumed to be located at $\boldsymbol{\rho}_0=(x_0, y_0)$ with a velocity $\boldsymbol{V}$ in the laboratory system such that $\rho_0=|\boldsymbol{\rho}_0|$ is the closest distance to the centre of rotation. Thus $\boldsymbol{V}=(-V_L y_0/\rho_0, V_L x_0/\rho_0)$ where both positive and negative values of V_L will be considered throughout the paper. The coordinates u and v in the rotating system are then given by

$$\begin{aligned} u &= \left(x_0-\frac{V_L y_0 t}{\rho_0}\right)\cos\omega t+\left(y_0+\frac{V_L x_0 t}{\rho_0}\right)\sin\omega t \\ v &= -\left(x_0-\frac{V_L y_0 t}{\rho_0}\right)\sin\omega t+\left(y_0+\frac{V_L x_0 t}{\rho_0}\right)\cos\omega t. \end{aligned} \tag{1}$$

With help of the expressions for the inertial forces and the scalar product between them

$$\begin{aligned} \boldsymbol{F}_{\mathrm{Cor}} &= 2m\left(\frac{V_L\omega}{\rho_0}\boldsymbol{\rho}_0-\omega^2\boldsymbol{\rho}\right) \\ \boldsymbol{F}_{\mathrm{cent}} &= m\omega^2\boldsymbol{\rho} \\ \boldsymbol{F}_{\mathrm{Cor}}\cdot\boldsymbol{F}_{\mathrm{cent}} &= 2m^2\omega^3(V_L\rho_0-\omega\rho^2) \end{aligned} \tag{2}$$

we can distinguish between three different types of trajectories shown in figure 1.

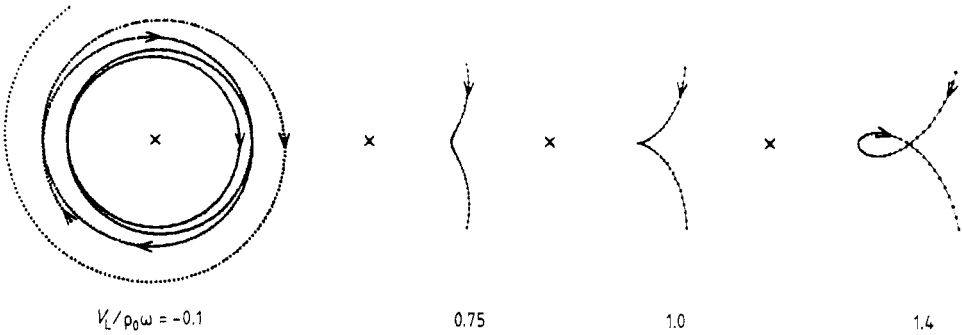

Figure 1. Parts of four trajectories in a rotating frame of a free particle. The centre of the rotation is marked with a cross in each case and the rotation is in the counterclockwise sense. The trajectories are denoted by the ratios $V_L/\rho_0\omega = -0.1$, 0.75, 1.0 and 1.4, where V_L is the velocity in the laboratory (fixed) frame, ρ_0 is the minimum distance to the centre of rotation and ω is the angular frequency. A negative value of V_L means that the direction of the angular momentum vector in the laboratory system is opposite to the direction of the angular frequency vector. Except for $V_L/\rho_0\omega = -0.1$ only a part of the trajectory close to ρ_0 is shown. For $V_L/\rho_0\omega < 0.5$ the Coriolis force and the centrifugal forces act in the opposite sense and the Coriolis force is stronger than the component of the centrifugal force perpendicular to the velocity vector in the rotating frame. For smaller velocities in the clockwise direction, $0.5 < V_L/\rho_0\omega < 1$ the inertial forces still act in the opposite sense but the centrifugal force can now dominate in the region where $\rho/\rho_0 < 3/\sqrt{8}$. If $V_L/\rho_0\omega = 1$ a branch point at the minimum distance is developed and for even larger values a loop exists. Within this loop the Coriolis force and the centrifugal force can act in the same direction.

(i) $\boldsymbol{F}_{Cor} \cdot \boldsymbol{F}_{cent} < 0$ and the curvature of the trajectory keeps a constant sign. This happens, because of the dominance of the Coriolis force, if $V_L/\rho_0\omega < 0.5$. The radius of curvature R_t of the trajectory at $\rho = \rho_0$ is then always greater than ρ_0 except for $V_L = 0$ where naturally $R_t = \rho_0$ (a circle in the clockwise sense); see figure 2.

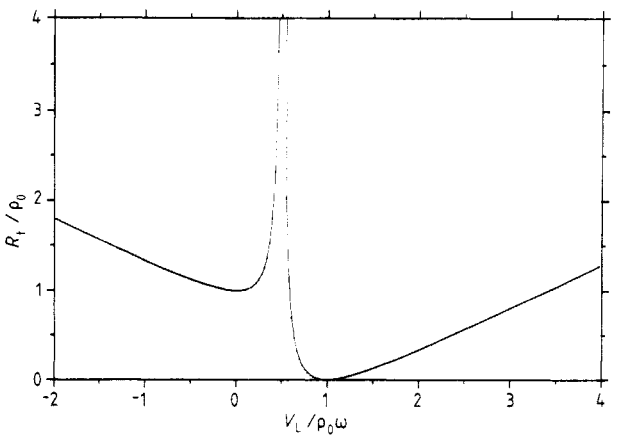

Figure 2. The radius of curvature of the trajectory, R_t, at the minimum distance to the centre of rotation, ρ_0, in units of ρ_0 as function of $V_L/\rho_0\omega$. For $V_L/\rho_0\omega = 0.5$ the two inertial forces cancel each other at ρ_0.

(ii) $\boldsymbol{F}_{\text{Cor}} \cdot \boldsymbol{F}_{\text{cent}} < 0$ and the centrifugal force can change the sign of the curvature in a small part of the trajectory. This occurs if $0.5 < V_L/\rho_0\omega < 1$. The change of curvature is produced whenever $\rho < \rho_0[3(V_L/\rho_0\omega) - 2(V_L/\rho_0\omega)^2]^{1/2}$. If $V_L = \rho_0\omega$ there is a branch point at the minimum distance to the centre of rotation and $R_t = 0$.

(iii) $\boldsymbol{F}_{\text{Cor}} \cdot \boldsymbol{F}_{\text{cent}} > 0$. The inertial forces act in the same direction in a certain region and a loop exists. This occurs if $V_L/\rho_0\omega > 1$ in the region where $\rho < \rho_0(V_L/\rho_0\omega)^{1/2}$.

The radius of curvature at $\rho = \rho_0$ is given by

$$R_t = \rho_0 \frac{(1 - V_L/\rho_0\omega)^2}{|1 - 2V_L/\rho_0\omega|}. \tag{3}$$

In the particular case when the particle goes through the origin ($\rho_0 = 0$) it is straightforward to show that the origin is always located on a loop which is present for any value of $V_L \neq 0$.

3. Motion within a rotating boundary

Consider a particle moving in two dimensions within a non-circular boundary and where the only forces acting on it are the inertial forces in equations (2). The boundary will in the following be characterised by the largest and smallest distance from the centre of rotation to the boundary, denoted $R_>$ and $R_<$ respectively, and the aspect ratio $\mu = R_>/R_<$. At the boundary the particle is supposed to be perfectly reflected. For a generic orbit the angular momentum is not conserved after a collision with the boundary. However, the Hamiltonian in the rotating system, H' (Landau and Lifshitz 1976)

$$H' = H - \omega l_z \tag{4}$$

where H and l_z denote the Hamiltonian and the angular momentum in the laboratory frame, respectively, provides a well known constant of motion. The term $-\omega l_z$ generates the two inertial forces. The constant value of H', in the following denoted e_ω, can in the laboratory system be expressed as

$$e_\omega = \tfrac{1}{2}mV_L^2 - \omega l_z = \tfrac{1}{2}mV_L^2 - m\omega\rho_0 V_L \tag{5}$$

or in the rotating system

$$e_\omega = \tfrac{1}{2}m(V_r^2 - \omega^2\rho^2) \tag{6}$$

where V_r denotes the magnitude of the velocity of the particle in the rotating system. For a given boundary the trajectories depend only on the ratio V_L/ω and it is therefore convenient to introduce the dimensionless parameter

$$\eta = \frac{e_\omega}{mR_>^2\omega^2} = \frac{1}{2}\left(\frac{V_L}{R_>\omega}\right)^2 - \left(\frac{V_L}{R_>\omega}\right)\frac{\rho_0}{R_>} = \frac{1}{2}\left[\left(\frac{V_r}{R_>\omega}\right)^2 - \frac{\rho^2}{R_>^2}\right]. \tag{7}$$

On each curve in the (ω, e_ω) plane with η constant the topologies of the Poincaré surfaces of section for a given boundary are the same (see figure 3 and § 5). Since $\rho \leqslant R_>$ equation (7) gives that $\eta \geqslant -0.5$. In the domain where $\eta < 0$ the orbit is confined within the boundary and a circle with radius $\rho_<$, where $\rho_< = R_>\sqrt{-2\eta}$. For $\eta = -0.5/\mu^2$ we have $\rho_< = R_<$. This circle, which always defines a forbidden region, does not touch the boundary for $-0.5/\mu^2 < \eta < 0$. If $\eta > 0$ no circle of confinement exists and the motion is possible everywhere within the boundary. The value $\eta = 0$ for which the

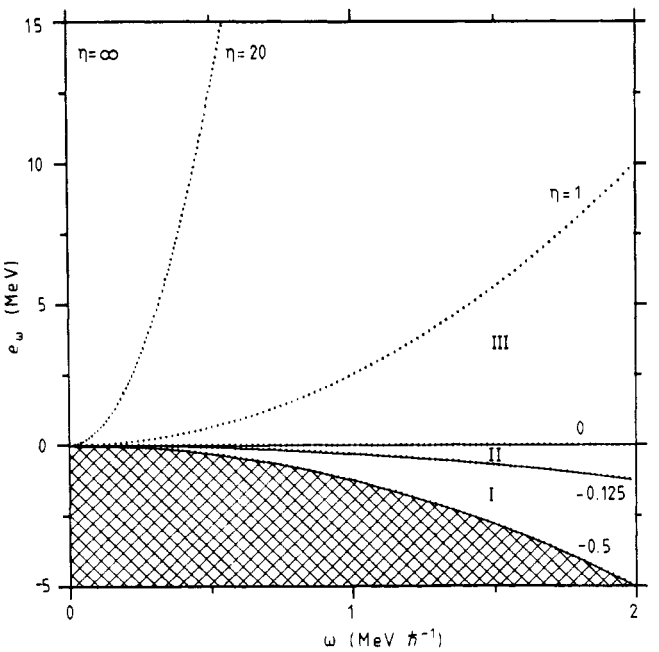

Figure 3. The constant of motion in the rotating frame, e_ω, as a function of ω. Some curves with a constant value of the dimensionless quantity $\eta = e_\omega / mR_>^2\omega^2$ are shown. The chosen units are appropriate for a rotating nucleus. The mass of the particle, m, is chosen as the proton mass and the largest distance from the centre of rotation to the boundary, $R_>$, is typical for an ellisoidal shape of a nucleus with mass number around 150 and $\mu = R_>/R_< = 2$ ($R_<$ is the smallest distance from the centre of rotation to the boundary). No motion is possible if $\eta < 0.5$ (hatched area). The available part of the (ω, e_ω) plane can be divided into three different regions which are separated by full curves. In region I ($-0.5 < \eta < -0.5/\mu^2$) the motion is only possible in separated domains while in region II ($-0.5/\mu^2 < \eta < 0$) the trajectory is confined within a circle, with radius $R_>\sqrt{-2\eta}$, and the boundary. In region III ($\eta > 0$) the motion is possible everywhere within the boundary.

kinetic and rotational energy are equal is thus the landmark of two different regimes and we will see in the following that the organisation of phase space is complex around this value. For orbitals around the Fermi level in a fast rotating heavy nucleus we have $\eta > 15$.

4. Trajectories in a rotating ellipse

To understand the Poincaré surfaces of section in § 5 we will consider the trajectories in an ellipse rotating in the counterclockwise sense with constant rotational frequency. Let us first consider the periodic trajectory between the two apices of the ellipse (points where $\rho = R_>$). In the non-rotating case this trajectory is the bouncing ball motion along the long diameter of the ellipse. In figure 4 a part of the periodic trajectory is shown in the laboratory system. At $t = 0$ the two apices are located at P and P' with the particle placed at P. After an elapsed time t the long diameter PP' has rotated an angle θ and the apices are then located at Q and Q'. If we want to find the particle at Q' the following condition must be fulfilled:

$$V_L / R_>\omega = -\cos(\theta/2)/(\theta/2) \tag{8}$$

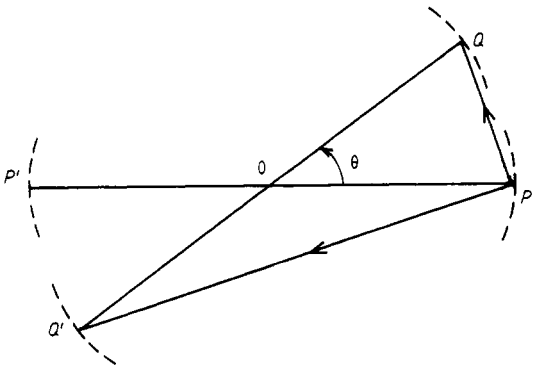

Figure 4. The position of the apices of an ellipse are shown at two different times. The particle may travel from P to Q (periodic trajectory on a single apex) or from P to Q' (periodic trajectory connecting the two apices).

remembering that both positive and negative values of V_L are considered (see § 2). Introducing this condition into the definition of η (7) gives

$$\eta = (1+\cos\theta)/\theta^2 + \sin\theta/\theta. \tag{9}$$

A periodic trajectory connected with a single apex is also possible if the self-intersection point of the loop (see the trajectory for $V_L/\rho_0\omega = 1.4$ in figure 1) lies at $\rho = R_>$. In this case we want to find the particle at Q instead (see figure 4) and therefore $V_L/R_>\omega = \sin(\theta/2)/(\theta/2)$ must be used in (7) which gives

$$\eta = (1-\cos\theta)/\theta^2 - \sin\theta/\theta. \tag{10}$$

An example of this periodic motion is shown at the right of figure 6(c). Just after the reflection with the boundary, the angle α between the velocity V_r and the positive tangent of the ellipse (pointing in the counterclockwise sense) is given by

$$\cos\alpha = \frac{(V_L/R_>\omega)^2 - 2\eta - 2}{2(1+2\eta)^{1/2}}. \tag{11}$$

This angle α will be used to define the Poincaré surfaces of section in § 5. The two functions in (9) and (10) are plotted in figure 5 where they are denoted by $\eta_{PQ'}$ and η_{PQ}, respectively. Obviously these equations provide only necessary but not sufficient conditions for the existence of the periodic trajectories since for $\mu > 1$ the particle will for suitable values of θ hit the boundary before it reaches Q or Q' (the dotted parts of the curves in figure 5 correspond to this event for $\mu = 1.25$). The discussion above can be repeated for the corresponding periodic trajectories at $\rho = R_<$, with some important differences, however. Obviously it is necessary to replace $R_>$ by $R_<$ and therefore the values of η given by (9) and (10) must be scaled. A periodic trajectory connected with the apex at the angle θ, or α, and for the value η will then be connected with the small axis at the same angle θ, or α, for a new value, η', given by $\eta' = \eta/\mu^2$. These periodic trajectories cannot intersect the ellipse and they exist for all values of μ and θ. In other words, the full curves represented in figure 5 which define η' can be used. Thus the curve corresponding to $\eta_{PQ'}$, denoted $\eta'_{PQ'}$ extends now in the interval $\eta' > -0.18/\mu^2$ while the loop at $\rho = R_<$ is possible when $-0.50/\mu^2 < \eta' < 0.29/\mu^2$. The bouncing ball motion along the small (long) axis is stable (unstable) for

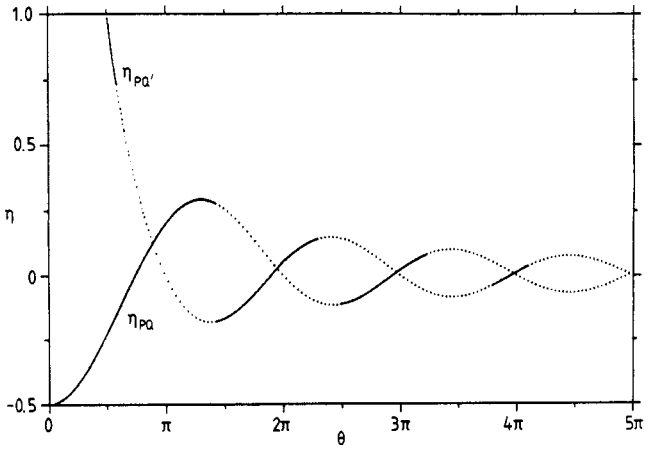

Figure 5. The curves labelled η_{PQ} and η_{PQ} are defined by equations (9) and (10), respectively, and give the set of η and θ values for which the periodic trajectories between the apices of the ellipse and at a single apex (loop) are possible. However, there is a possibility that the particle will hit the boundary before it reaches the apex and the dotted parts of the curves show when this occurs for an ellipse with $\mu = 1.25$. The figure can also be used for the corresponding periodic trajectories at $\rho = R_<$ if the η values in the figure are scaled with a factor $1/\mu^2$.

$\omega = 0$, while $\eta_{PQ} = -0.5$ ($\eta'_{PQ} = -0.5/\mu^2$) correspond to stable (unstable) points in phase space. Thus a shift of stability occurs from the short axis for large η to the apices for small η. This rearrangement mainly takes place in the region $-0.18/\mu^2 < \eta < 0.29$.

In order to obtain an orbit with counterclockwise motion in the rotating frame it is necessary that the trajectory is made by parts of the loop; see e.g. $V_L/\rho_0\omega = 1.4$ in figure 1. In this case the angular momentum for the orbit in the laboratory system, l_z, and in the rotating system is always positive ($\boldsymbol{l}_z \cdot \boldsymbol{\omega} > 0$). An example of counterclockwise motion is given at the right of figure 6(a). For $\eta < 0$ all orbits have $l_z > 0$ but consist of both clockwise and counterclockwise pieces; see figure 6(c). We will see in § 5 that the counterclockwise motion is to a large extent ordered. Especially, the orbit travelling along the boundary of the ellipse in this sense exists for all η values (see below).

Compared to the counterclockwise motion, the clockwise motion is more complex since many possibilities exist. For examples of clockwise motion see figure 6(a) (left and middle), parts of the trajectory of figure 6(b) (chaotic) and figure 6(c) (left). Let us now study the orbit travelling along the boundary in the clockwise sense. For a free particle with no boundary the radius of curvature, R_t, of the trajectory at the point $\boldsymbol{\rho}$ is given by

$$R_t = \frac{V_r^2}{2\omega V_r - \omega^2(\boldsymbol{\rho} \cdot \boldsymbol{n})} \tag{12}$$

where $\boldsymbol{n}$ denotes the outward normal of the trajectory. If the point defined by $\boldsymbol{\rho}$ is on the boundary a reaction is possible whenever R_t is greater than the radius of curvature, R_e, of the ellipse at $\boldsymbol{\rho}$. Observe that for the counterclockwise motion along the boundary a reaction of the boundary is always possible. After using (7) to eliminate V_r the

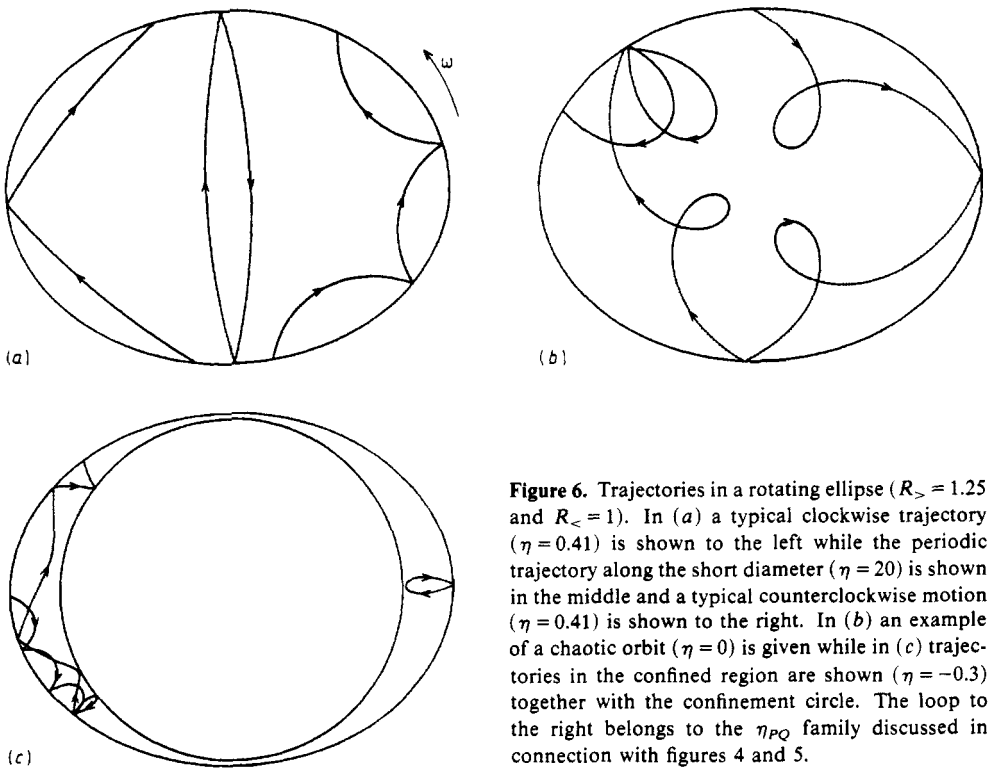

Figure 6. Trajectories in a rotating ellipse ($R_> = 1.25$ and $R_< = 1$). In (a) a typical clockwise trajectory ($\eta = 0.41$) is shown to the left while the periodic trajectory along the short diameter ($\eta = 20$) is shown in the middle and a typical counterclockwise motion ($\eta = 0.41$) is shown to the right. In (b) an example of a chaotic orbit ($\eta = 0$) is given while in (c) trajectories in the confined region are shown ($\eta = -0.3$) together with the confinement circle. The loop to the right belongs to the η_{PQ} family discussed in connection with figures 4 and 5.

condition $R_t > R_e$ is expressed as

$$4\eta^2 R_>^4 + 4\eta R_>^2[\rho^2 + R_e(\boldsymbol{\rho}\cdot\boldsymbol{n}) - 2R_e^2] + [(\rho^2 + R_e(\boldsymbol{\rho}\cdot\boldsymbol{n}))^2 - 4R_e^2\rho^2] > 0. \tag{13}$$

At the points on the boundary where $\boldsymbol{\rho}\cdot\boldsymbol{n} > R_e$ (or $R_>(1 - 1/\mu + 1/\mu^2)^{1/2} < \rho \leqslant R_>$) the condition is fulfilled for all values of η. If $\boldsymbol{\rho}\cdot\boldsymbol{n} < R_e$ the condition in (13) defines an interval in η in which the particle must fly away from the boundary at $\boldsymbol{\rho}$. The lower bound of this interval is greater than $-0.5(\rho/R_>)^2$. The minimum and maximum of the lower and upper bounds, respectively, of the intervals where the condition in (13) is not fulfilled gives the domain where the clockwise motion along the boundary is not possible. This interval is given by

$$\begin{aligned} &\eta_- < \eta < \eta_+ \\ &\eta_+ = -(1 + 1/\mu^2)/2 + \mu^2 + \mu\sqrt{\mu^2 - 1} \\ &\eta_- = \begin{cases} -(1 + 1/\mu^2)/2 + 4/3\sqrt{3}\mu & \text{if } \mu > 2/\sqrt{3} \\ -(1 + 1/\mu^2)/2 + \mu^2 - \mu\sqrt{\mu^2 - 1} & \text{if } \mu < 2/\sqrt{3} \end{cases} \end{aligned} \tag{14}$$

where $\eta_+ > 0$ and $\eta_- < 0$ for all values of μ (e.g. for $\mu = 1.25$, $\eta_+ = 1.68$ and $\eta_- = -0.20$). We will see in § 5 that the clockwise motion is to a large extent chaotic for $\eta_- < \eta < \eta_+$.

5. Poincaré surfaces of section

It is a common practice to represent the phase space of a system with two degrees of freedom by its Poincaré surface of section. For the surfaces of section we use the coordinate s/L, where s is the arc length from a point with $\rho = R_<$ to the impact point

(in the counterclockwise sense) and where L is the total length of the boundary, and the angle α which was defined in connection with equation (11). All information about the total surface of section is contained in the interval $0 \leqslant s/L \leqslant 0.25$ due to symmetry. In the non-rotating case the surface of section is also symmetric with respect to $\alpha = \pi/2$ while no specific symmetry is associated with the angle α in the rotating case since the time-reversal symmetry is broken. The orbits with $\alpha = 0$ and $\alpha = \pi$ describe the counterclockwise and clockwise motion along the boundary, respectively. A condition for the existence of the orbit with $\alpha = \pi$ was given by equation (13) for the ellipse. We will in this section discuss in detail the rotating elliptical billiard but, at the end, also consider the rotating stadium. The Poincaré section contains three different parts in the non-rotating elliptical case, which can be classified by the sign of a constant of motion, namely the scalar product of the two angular momenta, $\boldsymbol{l}_1$ and $\boldsymbol{l}_2$, with respect to the two foci of the ellipse (Berry 1981a). When $\boldsymbol{l}_1 \cdot \boldsymbol{l}_2 < 0$ the particle is able to cross the interval between the foci, while for $\boldsymbol{l}_1 \cdot \boldsymbol{l}_2 > 0$ it never crosses this interval. For $\boldsymbol{l}_1 \cdot \boldsymbol{l}_2 = 0$ the orbit crosses the foci and this value defines the separatrix. The manifold with $\boldsymbol{l}_1 \cdot \boldsymbol{l}_2 > 0$ is split into two disconnected submanifolds, occupying the same volume in phase space, corresponding to clockwise or counterclockwise motion around the foci.

A set of Poincaré surfaces of section is presented in figure 7 for an aspect ratio $\mu = 1.25$. The surface of section for $\eta = 20$ is very similar to the surface in the non-rotating case and the phase space is still roughly organised into three regions. Around the separatrix which existed in the non-rotating case ($\boldsymbol{l}_1 \cdot \boldsymbol{l}_2 = 0$) chaotic orbits now exist. With $\mu = 1.25$ in equation (14) we obtain that clockwise motion along the boundary is not possible if $-0.20 < \eta < 1.68$. As seen in figure 7, a large part of the clockwise motion is chaotic for the η values in this region while the counterclockwise motion remains ordered. The invariant curves around $s/L = 0$, 1 and 0.5, corresponding to orbits with $\boldsymbol{l}_1 \cdot \boldsymbol{l}_2 < 0$ in the non-rotating case, have disappeared for $\eta = 0.41$ although the periodic trajectory connecting the points with $\rho = R_<$ can exist for $\eta > -0.12$ (see § 4). However, a new zone of stability appears for $\eta = 0$ which is made of two disconnected parts near $s/L = 0.25$ and 0.75. The reason for this structure is the periodic trajectories that were described as the branch called η_{PQ} in figure 5 (i.e. the loops at $\rho = R_>$). These periodic orbits are present for $\eta < 0.29$. The clockwise motion along the boundary is again possible for $\eta = -0.3$ ($\rho = 0.97R_<$) and ordered motion appears in the upper part of the surface of section. For $\eta = -0.4$ two regions of confinement exist since $\rho_< = 1.12R_<$ and the phase space is invaded by invariant curves. The phase space of an ellipse with $\mu = 2$ is dominated in the non-rotating case by the orbits with $\boldsymbol{l}_1 \cdot \boldsymbol{l}_2 < 0$ (Arvieu and Ayant 1987a, b). As seen in figure 7, these invariant curves are replaced by chaotic dots in an interval around $\eta = 0$ and therefore we expect that the chaotic motion is more dominant for $\mu = 2$. This can also be seen in figure 8 for $\eta = 0.88$ and $\eta = -0.14$ ($\rho_< = 1.06R_<$). However, for $\eta = -0.42$ ($\rho_< = 1.83R_<$), which is smaller than $\eta_- = -0.24$, the invariant curves occupy the phase space.

We have also considered the case of a rotating stadium which is known to be completely chaotic in the non-rotating case (Berry 1981a). We present here the stadium for an aspect ratio $\mu = R_>/R_< = 1.25$. As seen in figure 9 invariant curves are obtained when η decreases. Most impressively the size of the chaotic area decreases with η. For $\eta = -0.14$ ($\rho_< = 0.66R_<$) the system has the same phase space organisation as the elliptical billiard with the loops at $s/L = 0.25$ and 0.75. For $\eta = -0.42$ ($\rho_< = 1.15R_<$) only invariant curves exist. For such a low value the circle of confinement crosses the boundary at a point where the latter is a circle and the particle is confined between

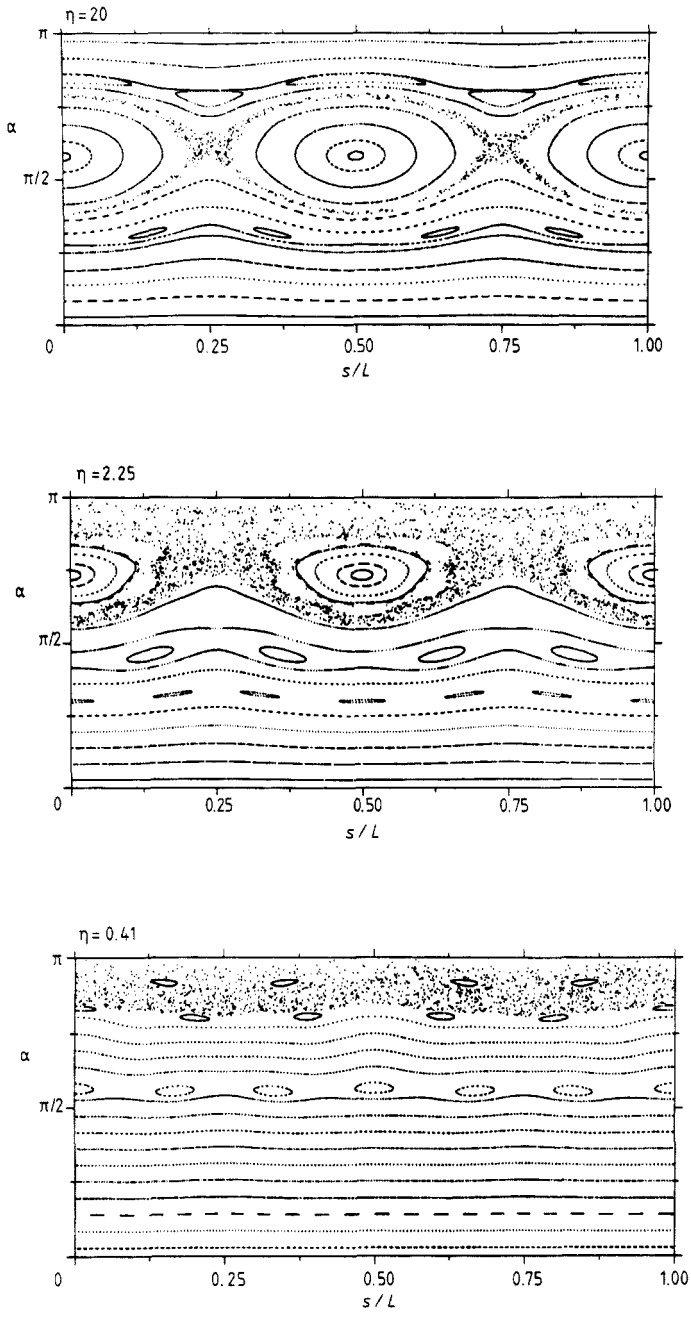

Figure 7. Poincaré surfaces of section of the rotating ellipse with $R_> = 1.25$ and $R_< = 1$ for different values of the parameter η as defined in equation (7). The two coordinates s/L and α are defined in § 5 and equation (11), respectively. To generate the surfaces 22 different orbits were considered and each orbit was iterated 400 times. The non-rotating ellipse is integrable. In the rotating case the occurrence of chaotic orbits is only dominant for the clockwise motion (upper part of the figures). Observe the change of stability from the short axis, $s/L = 0$, 1 and 0.5, for $\eta = 2.25$, to the long axis, $s/L = 0.25$ and 0.75, for $\eta = 0.0$.

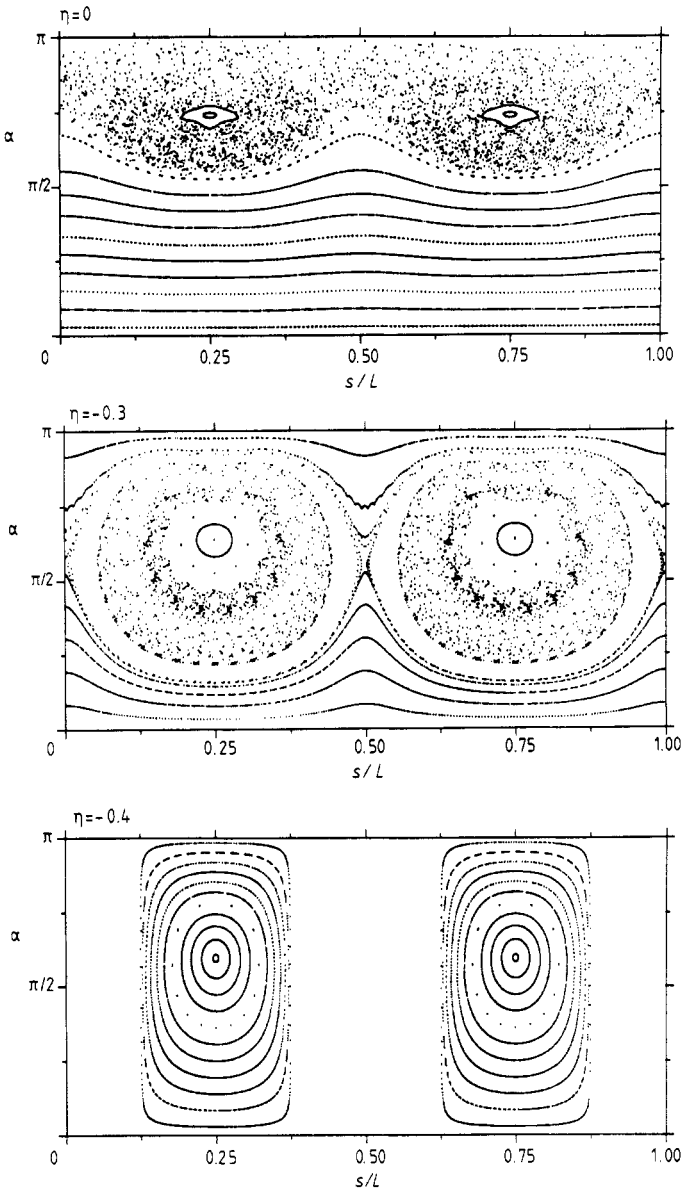

Figure 7. (continued)

two circles. This region is very similar to the corresponding region for the ellipse and explains why the two phase spaces become so similar when η is very low.

6. Discussion and conclusion

In summary, we have demonstrated by numerical methods that our rotating billiard is generic within the limits $\eta \to \infty$ and $\eta = -0.5$ where the phase space is reduced to two points. The organisation of phase space for the billiards in a Coriolis-centrifugal field and a constant magnetic field is found to be similar for weak fields but different

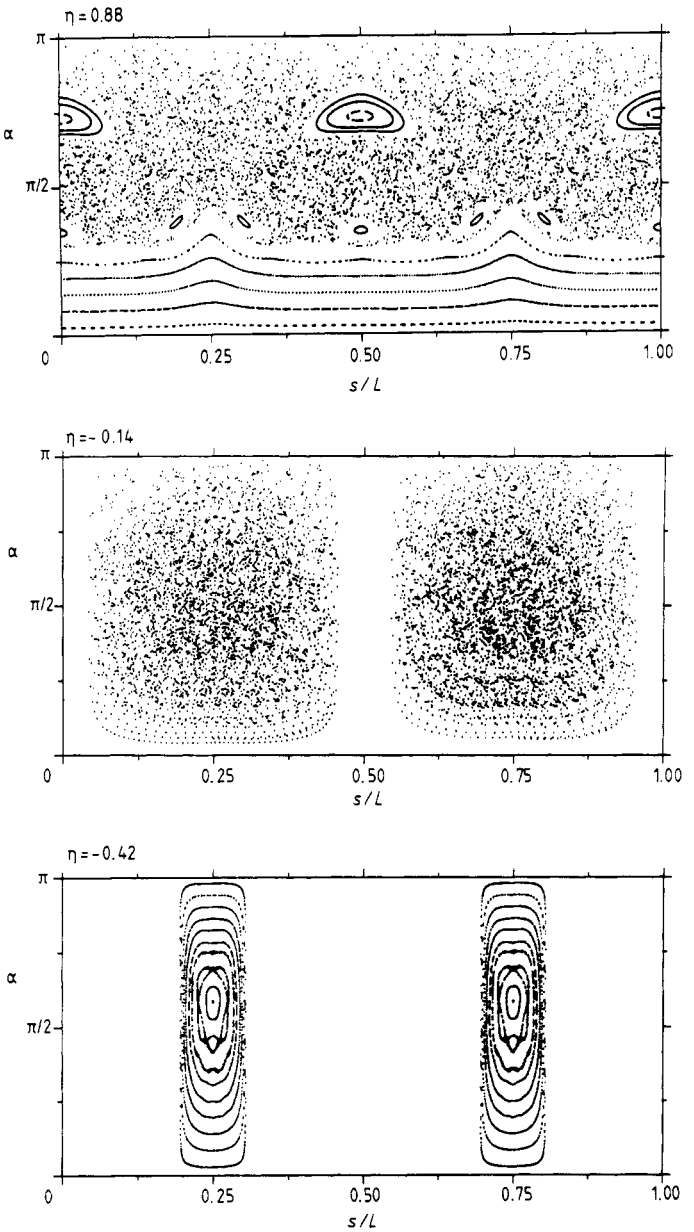

Figure 8. Same as figure 7 but for $R_> = 2$ and $R_< = 1$. The chaotic region is dominant for $\eta = 0.88$ and $\eta = -0.14$. However, the phase space organisation for $\eta = -0.42$ is similar to that for $\eta = -0.4$ in figure 7.

for strong fields. Chaos occurs in both systems when motion 'against' the rotation or the magnetic field along the boundary is impossible. Moreover, the stable counterclockwise motion is the counterpart to the adiabatic skipping motion discussed by Robnik and Berry. The removal of the zone of stability in the elliptical billiard is connected with the disappearance of the periodic motion along the short diameter together with the appearance of the stable loops at the apices.

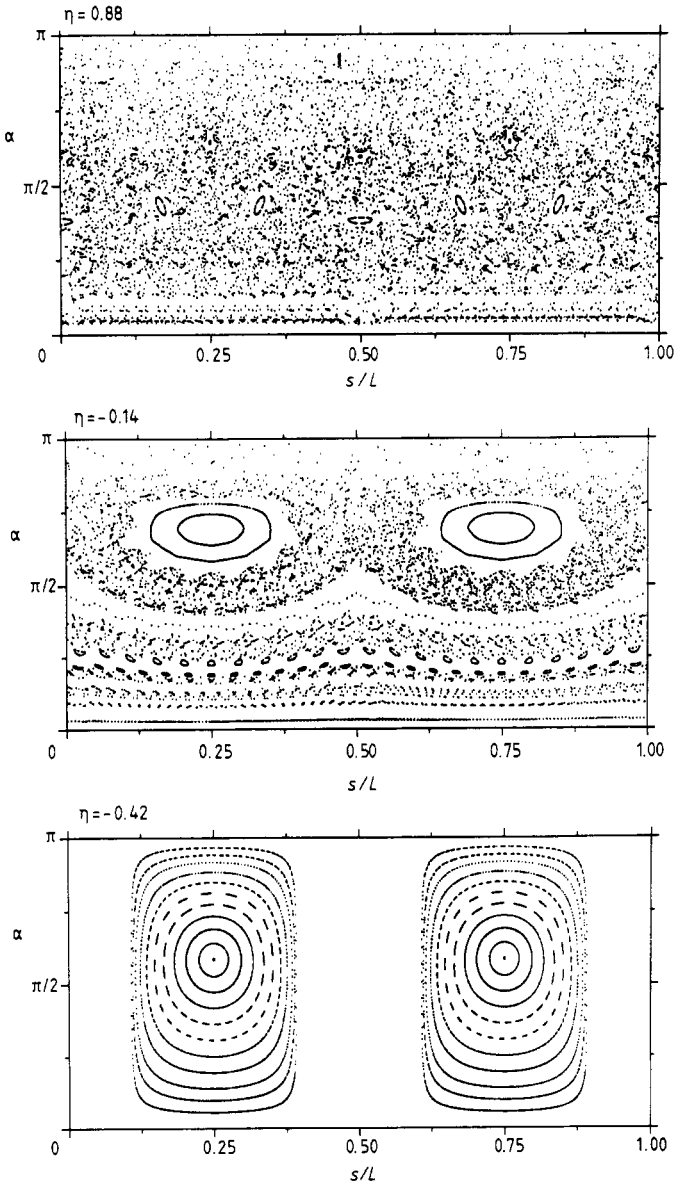

Figure 9. Same as figure 7 but for a rotating stadium with $R_> = 1.25$ and $R_< = 1.0$. The stadium is completely chaotic in the non-rotating case but when η decreases islands are created and the Poincaré surfaces for $\eta = -0.14$ and -0.42 are very similar to the surfaces for the rotating ellipse with the same axis ratio. Observe that for $\eta = -0.42$ the rotating stadium seems to be integrable.

From nearest-neighbour spacings of eigenenergies and Δ_3 statistics it has been claimed recently that the rotational motion is regular and has a stabilising effect on the particle motion (Abul-Magd and Weidenmüller 1985, Paar and Vorkapić 1988). Since $\eta > 15$ for the orbitals which contribute significantly to the angular momentum in a rotating nucleus we expect from our work that the rotational motion has only a

minor influence on the organisation of phase space. However, when $\eta \to -0.5$ the stabilising effect is nicely demonstrated in figures 7-9. It is known that a realistic deformed potential has chaotic orbits for $\omega = 0$ (Arvieu *et al* 1987). How the rotational motion will influence the three-dimensional case is not clear. Another interesting question concerns how the regular and chaotic motions influence the moment of inertia. Work on these questions is in progress.

Acknowledgments

We are strongly indebted to Dr Tord Bengtsson and his plotting routines. One of us (HF) is also grateful to the Swedish Research Council for a grant to visit Institute des Sciences Nucleaires, Grenoble, and be stimulated by the hospitality and the good working conditions there.

References

Abul-Magd A Y and Weidenmüller H A 1985 *Phys. Lett.* **162B** 223-6
Arvieu R and Ayant Y 1987a *J. Phys. A: Math. Gen.* **20** 397-409
—— 1987b *J. Phys. A: Math. Gen.* **20** 1115-36
Arvieu R, Brut F, Carbonell J and Touchard J 1987 *Phys. Rev.* A **35** 2389-408
Benettin G and Strelcyn J-M 1978 *Phys. Rev.* A **17** 773-85
Berry M V 1981a *Eur. J. Phys.* **2** 91-102
—— 1981b *Ann. Phys., NY* **131** 163-216
—— 1987 *Proc. R. Soc.* A **413** 183-98
Berry M V and Robnik M 1986a *J. Phys. A: Math. Gen.* **19** 649-68
—— 1986b *J. Phys. A: Math. Gen.* **19** 669-82
Birkhoff G W 1927 *Acta Math.* **50** 359
Bohr A and Mottelson B 1975 *Nuclear Structure* vol 2 (New York: Benjamin)
—— 1980 *Phys. Scr.* **22** 461-7
Christoffel K M and Brumer P 1986 *Phys. Rev.* A **33** 1309-21
Fairlie D B and Siegwart D K 1988 *J. Phys. A: Math. Gen.* **21** 1157-65
Heller E J 1984 *Phys. Rev. Lett.* **53** 1515-8
Henon M and Wisdom J 1983 *Physica* **8D** 157-69
Inglis D R 1956 *Phys. Rev.* **96** 1059-65
Keller J B and Rubinow S J 1960 *Ann. Phys., NY* **9** 24-75
Landau L D and Lifshitz E M 1976 *Mechanics* (*Course of Theoretical Physics* vol 1) (Oxford: Pergamon) 3rd edn
Lazutkin Y F 1973 *Izv. Acad. Sci. Ser. Math.* **37** 186-216
McDonald S W and Kaufman A N 1979 *Phys. Rev. Lett.* **42** 1189-91
—— 1988 *Phys. Rev.* A **37** 3067-86
Nakamura K and Thomas H 1988 *Phys. Rev. Lett.* **61** 247-50
Paar V and Vorkapić D 1988 *Phys. Lett.* **205B** 7-10
Robnik M 1983 *J. Phys. A: Math. Gen.* **16** 3971-86
—— 1984 *J. Phys. A: Math. Gen.* **17** 1049-74
Robnik M and Berry M V 1985 *J. Phys. A: Math. Gen.* **18** 1361-78
Sinai Ya G 1976 *Introduction to Ergodic Theory* (Princeton, NJ: Princeton University Press)